DOI: http://doi.org/10.4038/jgssl.v21i2.48

MICROSTRUCTURAL FEATURES OF GARNET PORPHYROBLASTS IN THE GRANULITE FACIES METAPELITES OF THE HIGHLAND COMPLEX OF SRI LANKA: EVIDENCE FOR A MULTIPLE GROWTH HISTORY OF GARNET AND EARLY DEVELOPMENT OF CRENULATION CLEAVAGE

V. MATHAVAN[1, 2 *]

[1] *Department of Geology, University of Peradeniya, Sri Lanka*

[2] *No 21 Gallipoli Place, Paraparaumu, 5032, Wellington, New Zealand (Present address)*

[*] *Corresponding Author: email- mathavan@xtra.co.nz*

(Received 4th January 2020; accepted 16th April 2020)

ABSTRACT

Inclusion-porphyroblast relationships reveal that the garnets in the metapelites of the Highland Complex (HC) of Sri Lanka have a multiple growth history. Garnets grew during a D2 phase of deformation coinciding with the development of crenulation cleavage and their growth reflects the prograde P-T-t path undergone by the HC. Garnet porphyroblasts in a group of schists enclose kyanite inclusion in the cores and they have a two-stage growth history. Their large inclusion-rich cores grew during early D2 deformation in the kyanite stability field enclosing straight, crenulated, and two sets of trails. Their inclusion-free rims grew during late- to post-D2 deformation in the sillimanite stability field. Straight inclusion trails represent the earliest recognizable fabric (S1) produced by a D1 deformation. Collectively these inclusion trails are the expression of a progressively developed crenulation cleavage, S1-S2. Breakdown of staurolite + muscovite led to the growth of inclusion-rich garnet cores with kyanite and staurolite inclusions. A late- to post-D2 increase of temperature produced sillimanite, and the growth of essentially inclusion-free garnet rims. Porphyroblastic garnets in another group of schists and gneisses have sillimanite inclusion in the cores and they have a protracted growth history spanning sillimanite-kyanite-sillimanite stability fields. Their inclusion-rich cores grew early in D2 deformation enclosing similar trail pattern as in the first group of schists but with sillimanite and fibrolite as the prominent trail-forming minerals. Growth of the outer core area of garnets followed enclosing rare staurolite and kyanite inclusions. Inclusion-free rims grew during late- to post-D2 deformation.

Keywords: *Highland Complex, Garnet porphyroblasts, Metapelites, Inclusion trails, Crenulation cleavage*

INTRODUCTION

Porphyroblasts often preserve key information on deformation and metamorphic evolution of rocks and thus play an important role in a wide range of metamorphic and structural studies (see Johnson, 1999; Johnson et al., 2006). Porphyroblasts often preserve trails of mineral inclusions that are remnants of linear and planar fabrics present in the rocks at the time of porphyroblast growth. Strong deformation and extensive recrystallization of the matrix after the growth of porphyroblasts may leave inclusion trails as the only record of the earlier structural history. Garnet porphyroblasts have been targeted for many microstructural studies as garnet is stable over a range of P-T conditions and its crystal structure accommodates a relatively large amount of foreign matter. Consequently, garnet can preserve inclusion assemblages and microstructures produced at different stages of metamorphism and deformation (e.g. Kim and Cho, 2008).

Inclusions in garnet porphyroblast may also include incompletely consumed reactant mineral/s and or product mineral/s produced by the porphyroblast forming reaction/s (e.g. Farber

et al., 2014). Moreover, the product mineral/s may be completely transformed (e.g. kyanite to sillimanite) and or consumed (e.g. biotite) by subsequent reaction/s in the matrix. In such instances, inclusions within porphyroblasts may be completely absent in the matrix. Relict minerals provide valuable information of about previous mineralogy, *P-T* evolution, and the reactions that produced the porphyroblasts. Relict mineral information locked up in garnet porphyroblasts has been successfully used to elucidate the early prograde *P-T* path in a number of granulite facies terranes, including those of the HC in Sri Lanka and South Harries in Scotland (e.g. Hiroi et al., 1994; Raase and Schenk, 1994; Baba, 1998; Dharmapriya et al., 2017).

Garnet-sillimanite schists are less dominant rock type in the HC but often they contain abundant porphyroblastic garnets, many of them with prominent inclusion trails. A textural variant of the schists, often referred to as 'khondalites' in the geological literature of Sri Lanka (Cooray, 1984), have large (1-3 cm) garnet porphyroblasts. The schists characteristically have an anhydrous mineralogy consisting mainly of garnet, sillimanite, K-feldspar, and quartz with or without plagioclase. Hydrous minerals are notably absent in the matrix but biotite, staurolite, kyanite, and hercynite occur as relict mineral within the garnet porphyroblasts (e.g. Hiroi et al., 1994).

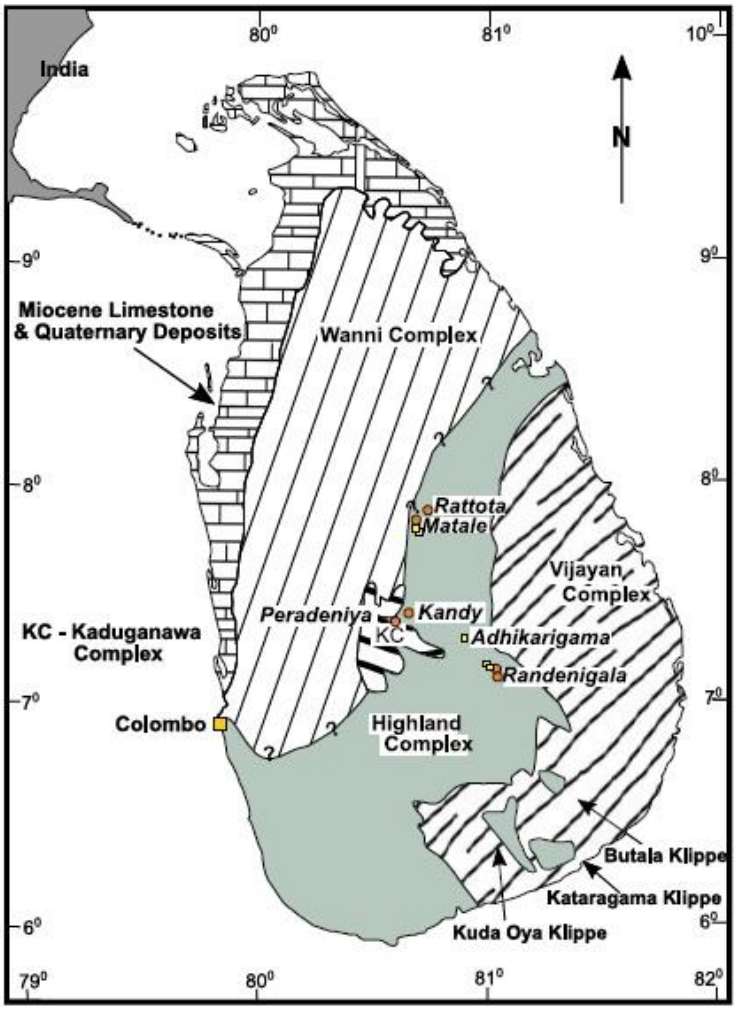

Fig. 1. *Map of Sri Lanka showing the boundaries of the Crustal Units delineated based on Nd model ages and the previously recognised geological units: The Highland Complex (HC), the Wanni Complex (WC), the Vijayan Complex (VC), and the Kadugannawa Complex (KC) (see text for details). Also shown is the distribution of Miocene limestone deposits, the locations of the studied samples (circles-group A samples and squares- group B samples), and the klippen of HC within the VC.*

Hiroi et al. (1987, 1994), who first recognised occurrences of these relict minerals in the pelitic schists and gneisses, suggested a clockwise prograde *P-T* path for the HC, going from the kyanite to sillimanite stability fields. Furthermore, Raase and Schenk (1994) reported relict kyanite being part of an inclusion sequence of sillimanite-kyanite- and sillimanite from the core to the rim of garnets in two pelitic rocks from the eastern HC and they suggested an extended *P-T* trajectory traversing sillimanite-kyanite-sillimanite stability fields for the eastern HC. However, this sequence of mineral inclusion where sillimanite inclusions predate kyanite inclusions is not confined to the eastern HC as initially thought by these authors. Dharmapriya et al. (2017) reported occurrences of similar inclusion pattern in khondalite samples from the central HC.

The previous microstructural studies on the high-grade rocks of Sri Lanka corroborated the evidence for a first phase of deformation D1, in the HC, that is largely obliterated by the intense D2 deformation (Berger and Jayasinghe, 1976; Kriegsman, 1991; Kehelpannala, 1997; Kröner et al., 1994b). Kehelpannala (1997) suggested that D2 deformation may have been associated with the development of crenulation cleavage and that in turn might have led to the formation of compositional layering in the metapelites. Recently, Ranaweera and Kehelpannala (2019) have documented the mesoscopic and microscopic structures in the sheared rocks associated with the Wanni Complex and Highland Complex boundary zone. The present study focuses on porphyroblast-inclusion microstructural features of porphyroblastic garnets in a group of garnet-sillimanite schist and gneiss samples collected from the north-central parts of the HC (see Figure 1). The objectives are to determine growth history of garnets and the relict minerals enclosed within garnets and to unravel the pre-granulite metamorphic and deformational history preserved within garnet porphyroblasts. Specially prepared, relatively large (6 x 4.5 cm and 7 x 2.5 cm) thin sections were used mostly in the present study.

GEOLOGICAL BACKGROUND

The high-grade basement rocks of Sri Lanka, which make-up about 90% of the surface of area of the island, comprise of three distinct crustal units delineated based on Nd model ages and the previously recognised geological units (Cooray, 1962,1994; Milisenda et al., 1988, 1994). These units are, the centrally located Highland Complex (HC) (model ages – 2.2-3.0 Ga), the Wanni Complex (WC) (1.1-2.0 Ga) on the west, and the Vijayan Complex (VC) (1.1-2.0 Ga) in the east (Figure 1). A much smaller unit known as the 'Kadugannawa Complex' (KC) originally mapped on lithology and the presence of doubly plunging synforms, has a similar range of Nd model ages as that of WC. The HC consists of an assemblage of closely associated and interlayered granulite facies rocks mainly of charnockitic gneisses, orthogneisses, and metasediments that include marbles, quartzites, pelitic gneisses, pelitic schists, and calc-silicate rocks. The pelitic schists commonly occur as small bands (5-15 m thick), closely associated with marble and quartzite. Rare UHT sapphirine granulites occur locally within the HC (see Dharmapriya et al., 2017 and the references therein). The WC is made of amphibolite to granulite facies rocks, mainly of charnockitic gneisses, granitic gneisses, migmatites and less abundant metasediments that include cordierite-bearing gneisses and it also hosts late- to post-tectonic granites. The geology of HC and WC has been reviewed by Mathavan et al. (1999). The VC, on the other hand, comprises predominantly granitic gneisses, migmatites, and minor metasediments of amphibolite facies although a recent field study by Kröner et al. (2013) has shown widespread occurrences of granulite facies assemblages that have been largely retrogressed and modified by migmatisation and K-metasomatism. Ranaweera and Kehelpannala (2019) interpreted the boundary between HC and WC as a shear zone as well as a suture zone.

An extensive *P-T* dataset obtained from conventional geothermobarometric calculations as well as petrogenetic grids and pseudosections are now available for both HC and WC rocks (Dharmapriya et al., 2017). The thermobarometry data suggest that the combined HC-WC is a tilted section of the lower-middle crust, with the *P-T* gradient increasing from 4.5-6.0 kbar and 700-750°C in the southwest to 8-9 kbar and 800-900°C in the east and southeast (Faulhaber and Raith, 1991; Raith et al., 1991; Schenk et al., 1991; Raase and Schenk, 1994; Schumacher et al., 2012). The rare UHT granulites within the HC recorded the peak metamorphic conditions of 9-12.5 kbar and 925-1150°C (Kriegsman and Schumacher, 1999; Sajeev and Osanai, 2004; Osanai et al., 2006; Dharmapriya et al., 2015). The estimated peak

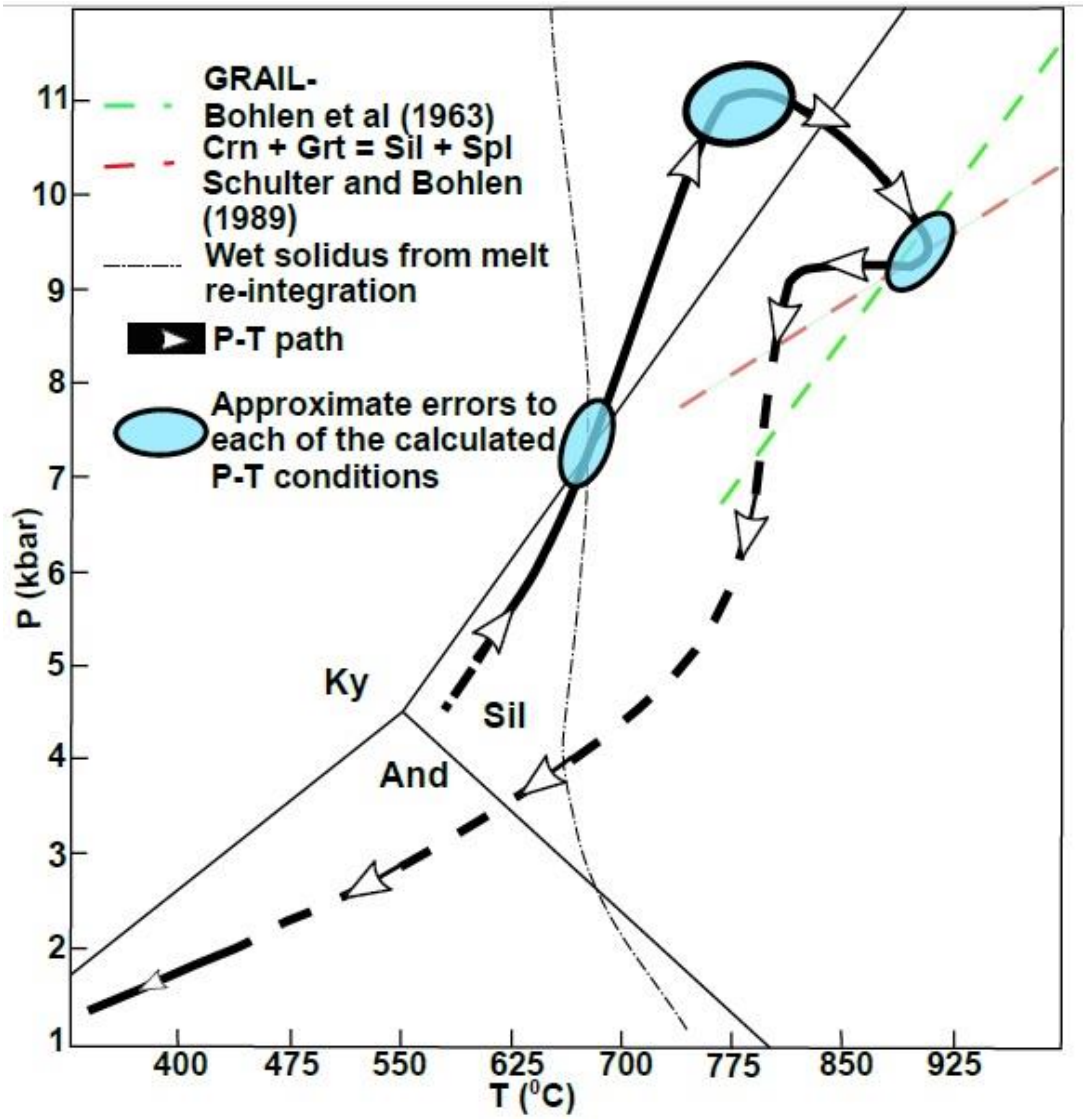

Fig. 2. *P-T diagram outlining the shape of the P-T-t path inferred for the HC (after Dharmapriya et al., 2017). The group (A) samples of the present study record mineral inclusion evidence for the upper part of the prograde P-T-t path shown here, going from kyanite to sillimanite stability fields whereas the group (B) samples record evidence for a protracted path traversing sillimanite-kyanite-sillimanite stability field (see text for details).*

P-T conditions for the VC are ca. 8 kbar and 800-850°C (Kleinschrodt, 1994).

The detailed aspect of the *P-T-t* path followed by granulites of the HC is debated (Dharmapriya et al., 2017; He et al., 2018 and references therein). Nevertheless, it includes a history that includes a protracted clockwise segment from the sillimanite to the kyanite stability field, a prograde decompression segment (transition from kyanite to sillimanite field), and a near isobaric cooling segment subsequent to peak metamorphism in the sillimanite field, followed by a near isothermal decompression and uplift, ending with the final uplift and cooling in the andalusite field. The *P-T-t* path derived for the HC by Dharmapriya et al. (2017) is shown in Figure 2. Extensive isotopic studies have established that the age of high-grade metamorphism in all three crustal units is bracketed to 530-600 Ma (e.g. Hölzl et al., 1991, 1994; Kröner et al., 1994a; Santosh et al., 2014; Dharmapriya et al., 2016 and

others). The UHT granulites, once thought to be exotic blocks (see Mathavan et al., 1999), now have a revised metamorphic age of ca. 540 Ma (see Sajeev et al., 2010). Subduction-related collisional tectonic models linked to the assembly of Gondwana have been proposed to explain how these distinct crustal units were brought together as a single landmass (Kehelpannala, 2004; Santosh et al., 2014; He et al., 2016; Touret et al., 2019).

STRUCTURAL FRAMEWORK

Berger and Jayasinghe (1976) initially established the poly-phase deformational feature of the HC (then known as the Highland Series) and their structural framework formed the basis for the subsequent workers to elaborate and expand the scheme (Kehelpannala, 1997, 2003). There are two strong and prominent structural features shown by the HC rocks: 1) the strong linear and planar fabrics associated with the prominent lithological layering and 2) km scale open to tight upright folds that largely determine the topography of the central highlands. Berger and Jayasinghe (1976) ascribed the main L-S fabric to D1 and D2 deformational phases formed under granulite facies conditions and the subsequent workers to a large degree accepted the inferences (see Table 1 in Kehelpannala, 1997, 2003). However, there is microstructural evidence available now suggesting the metamorphic condition during D1 was amphibolite facies (e.g. Kehelpannala, 1997) and not granulite facies as thought previously (e.g. Berger and Jayasinghe 1976).

Many workers (e.g. Yoshida et al 1990; Almond 1994), including Berger and Jayasinghe (1976), concluded that the D3 phase of deformation formed the major upright folds. However, Kehelpannala (1997, 2003) recognised two additional phases of deformation, D3 and D4, before the upright folds formed by D5 deformation and the author defined an additional, D6 phase of deformation as well, inferred from local refolding of major upright folds. Furthermore, Kehelpannala (1997, 2003) suggested two phases for the D2 deformation; 1) the first phase was linked to the development of crenulated inclusion trails in garnets, 2) the second phase was considered as non-coaxial deformation responsible for partial post-growth rotation of garnets in metapelites and the development of the major compositional layering associated with S2.

The timing of the development of crenulated trails in garnets and the post-growth rotation of garnet porphyroblasts are re-examined in the present study.

MICROSTRUCTURAL FEATURES-OBSERVATIONS

MATRIX

The matrix of schists that hosts porphyroblastic garnets is fine- to -medium-grained (1-2 mm) and has a moderate to strong schistose foliation, S2, defined by dimensionally aligned long prismatic sillimanite, and elongate to ribbon quartz grains (Figure 4a, 4h). In places, ilmenite, rutile, and graphite also contribute to the foliation. Biotite is part of the foliation in the gneisses. The schistose foliation is a composite foliation (S_c) developed from reoriented and transposed S1, newly formed S2, and possibly S0 (see later). It frequently wraps around the garnet porphyroblasts and pressure shadows formed by coarse equant quartz and K-feldspar grains are present in places (Figure 5c). Granoblastic texture is dominant in parts of the matrix where basal and short prims of sillimanite, K-feldspar and equant quartz grains are abundant. Furthermore, clusters and patches of sillimanite occur in places and some of the clusters have subidioblastic shapes. Rarely, matrix quartz grains include dimensionally aligned sillimanite grains and the reverse relationship is observed as well. Matrix quartz and other minerals, particularly sillimanite and garnet, in places have a film of perthitic feldspar around or partly around them (see documentation by Hiroi et al. 1997) and a similar perthitic feldspar film occurs between quartz inclusions and their host garnets.

GARNET PORPHYROBLASTS-GROUP A SAMPLES

The studied samples are divided into two groups, A and B, based on the type of inclusion minerals present in the cores of garnet porphyroblasts. Sillimanite and or fibrolite are absent in the cores of the garnets in-group A samples, but may occur at the rims whereas garnets in-group B samples that include the gneisses, commonly have sillimanite and or fibrolite inclusions in the cores and they may be present in the rims too. The term ‘fibrolite’ is used here for the fine acicular variety of Al_2O_5. Fibrolite occurs exclusively as inclusions within

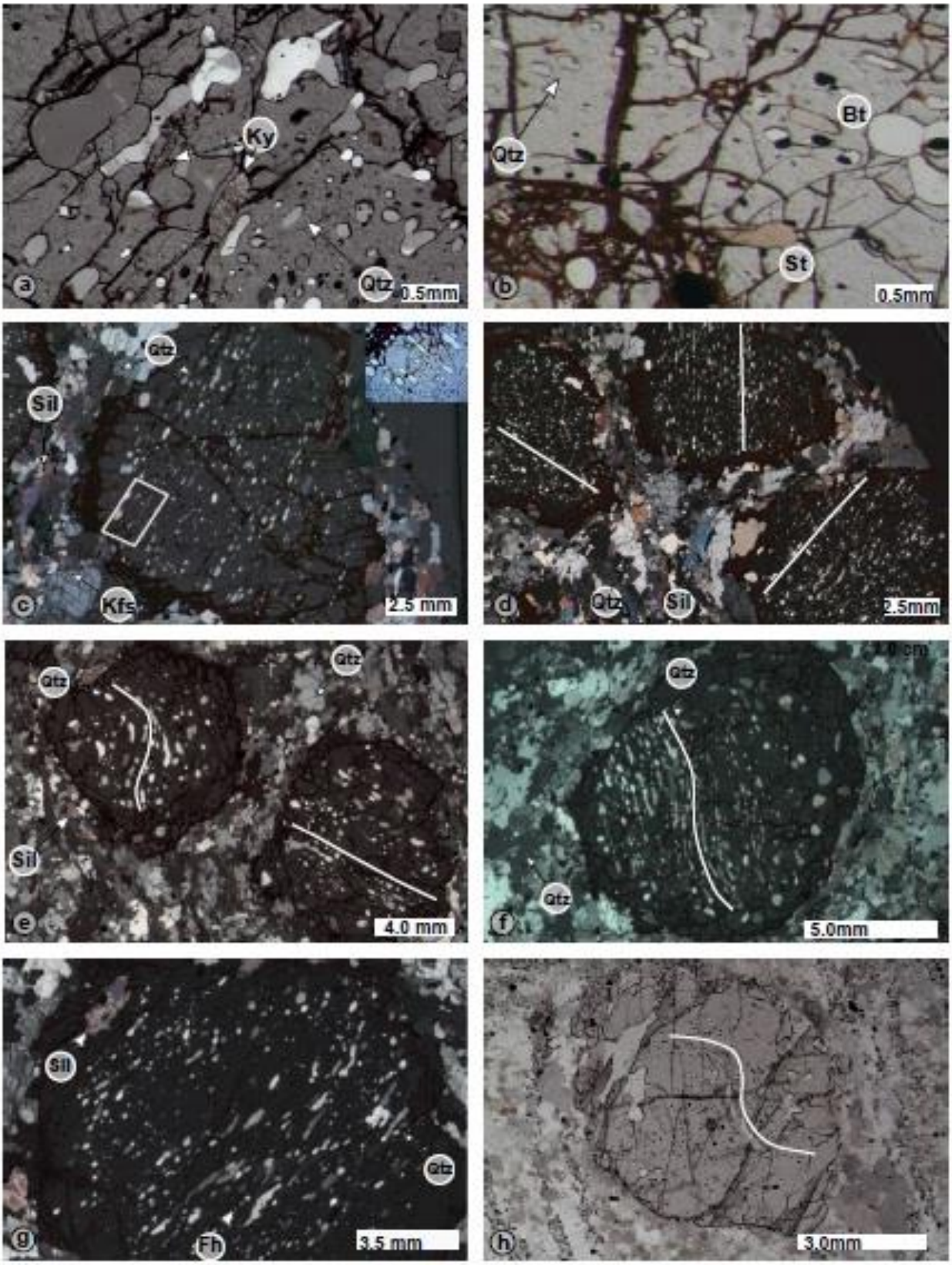
Ky
Qtz
a
0.5mm
Bt
Qtz
St
b
0.5mm
Qtz
Sil
c
Kfs
2.5 mm
d
Qtz
Sil
2.5mm
Qtz
Qtz
Sil
e
4.0 mm
Qtz
Qtz
f
5.0mm
Sil
Qtz
g
Fh
3.5 mm
h
3.0mm

Figure 3.

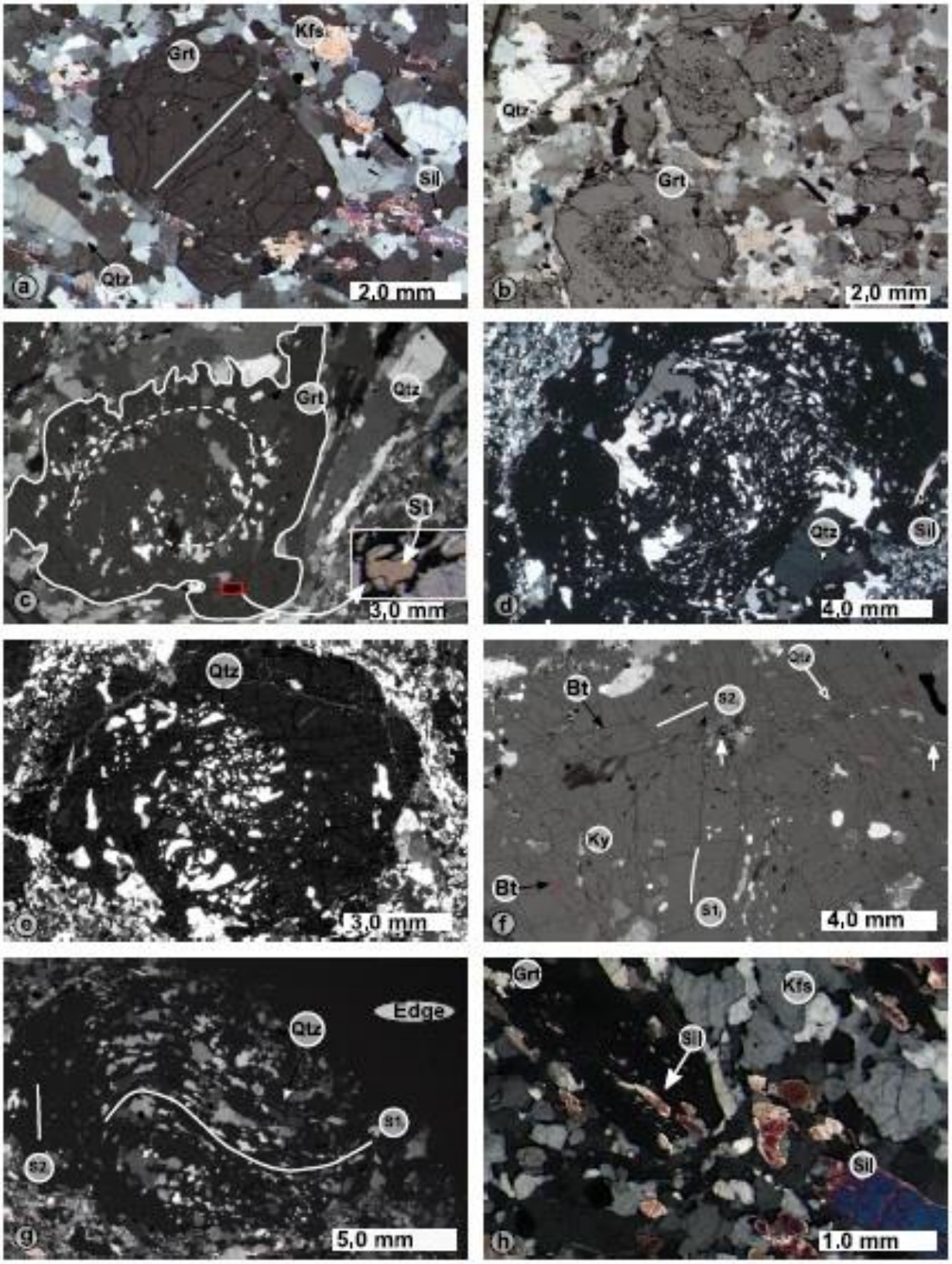
Grt
Kfs
Sil
Qtz
a
2,0 mm
Qtz
Grt
b
2,0 mm
Grt
Qtz
St
c
3,0 mm
Qtz
Sil
d
4,0 mm
Qtz
e
3,0 mm
Bt
Sz
Ky
Bt
Si
f
4,0 mm
Edge
Qtz
Si
Sz
g
5,0 mm
Grt
Kfs
Sil
Sil
h
1.0 mm

Figure 4.

garnets. The size and shape of the garnets vary among the samples. Garnet porphyroblasts (0.7 – 3.0 cm) with subidioblastic to sub-rounded shapes are common in the khondalites whereas 3-4 mm subidioblastic to xenoblastic microporphyroblasts (referred as porphyroblasts here for simplicity) are common in the other schist samples. Few garnet grains are elongate parallel to the matrix fabric (Sc). In addition, a few small (1-2 mm) garnets may occur along with the porphyroblastic garnets and the inclusion pattern in them contrasts with those of the porphyroblastic garnets (see later). Inclusions are abundant in most garnets and they often define prominent trails although nearby and side-by-side garnets may be free of inclusions or have non-oriented inclusions. The inclusion trails consist mainly of dimensionally aligned quartz, and ilmenite and lesser amounts of apatite, rutile, and monazite. Rare biotite, staurolite, kyanite, and hercynite occur exclusively within porphyroblastic garnets as relict minerals (Table 1). The relict mineral grains may align and form part of the inclusion trails (Fig. 3a, b) but often they occur as non-oriented grains. The other minerals that may be present as inclusions are graphite, corundum, plagioclase, and K-feldspar. The inclusions are generally small (<0.2 mm) and very much smaller than the corresponding matrix minerals indicating a major coarsening of matrix grains after the growth of the garnets (Fig. 3c-f & Fig. 4a, c). Quartz is the most abundant inclusion mineral and its shape varies locally but elliptical and elongate grains with sub-rounded corners are predominant (Fig. 3c-g & Fig. 4 g). Thin discontinuous layers of quartz grains are present in a few garnets. In a few instances, staurolite inclusions show reaction relationships: surrounded by hercynite or a combination of kyanite, hercynite, and opaque (Fig. 4c). However, kyanite-quartz and biotite-quartz inclusion pairs coexist stably (see Table 1)

Fig. 3*. Photomicrographs of garnet porphyroblasts in-group A schists showing microstructural features of inclusion trails, core-rim relationships, and relict inclusion minerals. (a) Relict kyanite inclusions (arrowheads) dimensionally aligned along with the weakly aligned quartz inclusions;* ***partly crossed polars (PCP)****; (sample 2). (b) Relict staurolite and biotite inclusions partly dimensionally aligned with straight trails of quartz and opaques;* ***PCP****; (4). (c) Large core of a garnet porphyroblast containing straight trails of quartz and some opaques that are very strongly dimensionally oriented; the inset shows elongate quartz grains;* ***XP (crossed polars)*** *;(4). (d) Adjacent garnet porphyroblasts with straight inclusion trails that are diversely oriented; the garnet in Fig.3c is here on top right of the microphotograph; note the contrasting size of the inclusion and the matrix minerals;* ***PCP****; (4). (e) Two adjacent garnet porphyroblasts with different trail geometries in the cores; one contains crenulated trails (top) and the other has moderately defined straight inclusion trails; note small inclusion-free rims in both garnets;* ***XP****; (2). (f) Gently crenulated but strongly dimensionally oriented inclusion trails in a garnet porphyroblast; note the trails are strongly discordant to the matrix fabric (upper left);* ***XP****; (2). (g) Inclusions in a garnet porphyroblast form mostly straight trails that are axial planner to a microfold hinge; Note coarse sillimanite grains at the rims;* ***XP****; (4). (h) Inclusion trails at the garnet porphyroblast core define sigmoidal pattern;* ***PCP****; (11).*

Fig. 4. *Photomicrographs of garnet porphyroblasts and microporphyroblasts in-group A schists showing microstructural features of inclusion trails, and core-rim relationships. (a) Garnet microporphyroblast containing straight inclusion trails mainly of fine quartz and opaques and the trails are strongly discordant to the matrix fabric S2 defined by elongate quartz, sillimanite, and opaques;* ***XP****; (9). (b) Cores of three garnet microporphyroblasts contain weakly oriented inclusion trails and their rims are free of inclusions;* ***PCP****; (8); (c) Garnet porphyroblast with a large core containing spiral shaped inclusion trails (SSITs); the inset shows partial replacement of staurolite by spinel and opaque;* ***CP****;(6). (d) Garnet porphyroblast with a large core-containing spiral shaped inclusion trails; note coarse quartz inclusions at the opposite sides, near the rims;* ***XP****; (5). (e) Garnet porphyroblast core contains possibly two sets of SSITs* ***XP****; (1). (f) Garnet core containing two sets of inclusion trails that partly resemble S1-S2 differentiated crenulation cleavage; weakly crenulated trails ($S1_i$) at the centre are made of quartz, opaques, kyanite, biotite, staurolite; the second set of trails ($S2_i$) is straight and consists of opaques, biotite, quartz; secondary sillimanite grains (arrow heads)after garnet also present;* ***PCP****; (3). (g) Garnet porphyroblast containing two sets of trails that partly resemble S1-S2 differentiated crenulation cleavage; the curved trails ($S1_i$) at core consisting mainly of quartz end abruptly near the rim; the weakly defined straight trails (S2i) near the rim is oblique to the curved trails at core;* ***XP****;(3). (h) A small garnet containing straight trails of sillimanite and fibrolite and the trails are parallel the coarser matrix fabric defined mainly by elongate sillimanite;* ***XP****; (3).*

Table 1. *Mineralogy and sample locality of selected khondalites, schists and gneiss.*

Ref. No	Field No	Locality	Peak assemblage	Inclusion minerals	Rock type	Group
1	P1	Peradeniya	Grt-Sil-Kfs-Qtz	Qtz, Ilm, Sil, Bt*, Ky*, (Bt*-Qtz), St*	Khondalite	A
2	55, 55A	Kandy	Grt-Sil-Kfs-Qtz	Qtz, Ilm, Sil, Ky*, (Ky*-Qtz), Ap, Mnz, Rt	Khondalite	A
3	607, 607A	Hantana, Kandy	Grt-Sil-Kfs-Qtz	Qtz, Pl, Bt*, St*, Spl*, Ky*, (Ky*-Spl*), (Ky*-Bt*), (Bt*-Qtz)	Khondalite	A
4	630, 630A	Rattota	Grt-Sil-Kfs-Qtz	Qtz, Ilm, Sil, Ky*, (Ky*-Bt*), Bt*, (Bt*-Qtz), St*, Ap, Mnz, Rt	Khondalite	A
5	602	Akurutale, Randenigala	Grt-Sil-Kfs-Qtz	Qtz, Ilm, Bt*, St*, Mnz, Fi, Rt, Kfs	Khondalite	A
6	632A	Matale	Grt-Sil-Kfs-Qtz-Pl	Qtz, Ilm, Ap, St*, Spl*, Ky*-Cor, Bt*	Khondalite	A
7	202	Adhikarigama	Grt-Sil-Kfs-Qtz	Qtz, Ilm, Sil, Fi, Mnz, Rt, Spl, Bt*	Schist	B
8	622	Lesmoir estate, Kegalle	Grt-Sil-Kfs-Qtz	Qtz, Ilm, Pl, Bt*, Sil, Fi, Spl*, Ap	Schist	A
9	632B, 632C	Matale	Grt-Sil-Kfs-Qtz-Pl	Qtz, Ilm, Sil, Bt*, Ap, Spl*, (Ky*-Spl*), Rt	Schist	B
10	631	Matale	Grt-Sil-Kfs-Qtz	Qtz, Sil, Ky*, St*, Bt*, Fi, Spl*, Rt, Ap	Schist	B
11	616	Akurutale, Randenigala	Grt-Sil-Kfs-Qtz	Qtz, Ilm, Sil, Bt*, Fi, Rt, Kfs	Schist	A
12	604	Hattumuna, Randenigala	Grt-Sil-Kfs-Qtz-Pl-Bt	Qtz , Ilm, Sil, Bt, Ky*, Gr, Fi	Gneiss	B
13	605	Hattumuna, Randenigala	Grt-Sil-Kfs-Qtz-Pl-Bt[1]	Qtz , Ilm, Sil, Fi, Bt, Gr, Rt	Schist	B

Abbreviation follows Kretz (1983), Fi -Fibrolite, * Relict mineral, [1]Retrograde, Ref No = sample reference numbers used in the text and Figure 1.

Table 2. *Representative microprobe analyses of garnet.*

Sp. Ref. no	5	5	3	3	4	4	**4	9	9	10	10	13	13
Position	rim	core	rim	core	rim	core	rim	rim	core	rim	core	rim	core
Type	Khondalite (Schist A)							Schist A		Schist B		Gneiss	
Inclusion	free	rich	free	rich	-	-	-	free	rich	free	rich	free	rich
SiO_2	36.92	36.68	36.88	36.55	38.35	37.78	37.54	37.80	37.87	37.70	37.28	39.19	38.84
TiO_2	0.03	0.03	0.06	0.03	0.04	0.04	0.02	0.00	0.01	0.17	0.01	0.02	0.01
Al_2O_3	21.15	21.15	21.01	21.17	21.62	21.45	21.67	21.56	21.39	21.68	21.29	22.18	22.11
*Fe_2O_3	0.03	0.00	0.26	0.00	0.26	0.32	0.00	0.24	0.39	0.00	0.16	0.12	0.07
MgO	3.45	3.46	3.51	3.49	6.68	6.29	6.83	7.12	6.92	6.57	6.22	9.98	10.02
CaO	0.98	0.92	1.37	1.43	2.48	2.93	1.29	1.31	1.47	0.56	0.64	1.42	1.64
MnO	0.45	0.44	0.35	0.37	0.37	0.40	0.34	0.47	0.44	0.45	0.40	0.63	0.59
FeO	37.55	37.85	37.07	36.50	30.86	31.00	32.19	31.68	31.49	33.47	33.52	27.02	26.67
ZnO	0.04	0.00	0.19	0.00	0.08	0.07	0.02	0.12	0.08	0.00	0.04	0.01	0.01
Total	100.60	100.54	100.71	99.54	100.74	100.29	99.90	100.31	100.06	100.61	99.56	100.55	99.95
Cation/ oxygen	12	12	12	12	12	12	12	12	12	12	12	12	12
Si	2.967	2.955	2.962	2.961	2.987	2.968	2.960	2.965	2.977	2.966	2.968	2.990	2.981
Ti	0.002	0.002	0.004	0.002	0.003	0.002	0.001	0.000	0.001	0.001	0.001	0.001	0.001
Al	2.005	2.008	1.989	2.021	1.985	1.986	2.014	1.993	1.981	2.010	1.997	1.994	2.000
Fe^{+3}	0.002	0.000	0.016	0.000	0.015	0.019	0.000	0.014	0.023	0.000	0.009	0.007	0.004
Mg	0.413	0.415	0.420	0.422	0.775	0.737	0.803	0.833	0.811	0.770	0.738	1.135	1.146
Ca	0.084	0.079	0.118	0.124	0.207	0.247	0.109	0.110	0.124	0.047	0.055	0.116	0.135
Mn	0.031	0.031	0.024	0.025	0.025	0.027	0.022	0.031	0.029	0.030	0.027	0.041	0.038
Fe^{+2}	2.520	2.550	2.489	2.473	2.010	2.037	2.122	2.078	2.070	2.202	2.231	1.724	1.712
Zn	0.003	0.000	0.012	0.000	0.005	0.004	0.001	0.007	0.005	0.000	0.003	0.000	0.001
Total	8.029	8.039	8.033	8.027	8.011	8.027	8.032	8.032	8.020	8.028	8.029	8.008	8.017
Mg/Mg+Fe	0.14	0.14	0.14	0.15	0.28	0.27	0.27	0.29	0.28	0.26	0.25	0.40	0.40
Almandine	82.73	82.94	81.64	81.27	66.67	66.86	69.45	68.09	68.24	72.22	73.14	57.18	56.48
Pyrope	13.55	13.51	13.77	13.85	25.71	24.19	26.27	27.29	26.73	25.26	24.19	37.63	37.82
Grossular	2.58	2.49	2.93	4.00	5.97	7.08	3.52	2.89	2.90	1.50	1.31	3.47	4.23
Spessartine	1.00	1.00	0.78	0.83	0.82	0.88	0.73	1.02	0.97	0.99	0.89	1.35	1.26
Andradite	0.14	0.05	0.87	0.05	0.84	0.99	0.03	0.71	1.16	0.03	0.48	0.36	0.21
Total	100.00	99.99	99.99	100.00	100.01	100.00	100.00	100.00	100.00	100.00	100.01	99.99	100.00

*calculated ** small garnet

Table 3. *Representative microprobe analyses of inclusion (within garnet) and matrix minerals (nd. not determined).*

Mineral	kyanite		sillimanite			staurolite		biotite		kfs	plagio
Sp. Ref. No	3	4	4	3	4	4	4	7	13	4	4
Type	inclusion	inclusion	inclusion	matrix	inclusion	inclusion	inclusion	inclusion	matrix	matrix	matrix
SiO_2	36.45	36.55	37.35	36.01	36.31	24.89	24.72	36.96	37.54	66.13	60.70
TiO_2	0.03	0.01	0.00	0.02	0.03	1.34	1.73	6.53	5.90	nd	nd
Al_2O_3	62.54	62.76	62.19	62.34	62.53	57.28	56.98	15.87	15.15	18.57	25.54
MgO	nd	nd	nd	nd	nd	2.37	2.50	12.30	15.23	0.00	0.00
CaO	nd	nd	nd	nd	nd	nd	nd	0.01	0.00	0.16	5.63
MnO	nd	nd	0.02	nd	nd	nd	nd	0.00	nd	nd	nd
FeO	0.28	0.49	0.52	0.38	0.34	11.10	11.22	10.68	8.96	0.01	0.00
ZnO	nd	nd	0.11	0.08	0.03	1.73	1.50	0.05	0.10	nd	nd
Na_2O	nd	nd	nd	nd	nd	nd	nd	0.47	nd	1.99	8.26
K_2O	nd	nd	nd	nd	nd	nd	nd	8.79	9.28	12.28	0.15
H_2O	nd	nd	nd	-	nd	1.09	1.09	3.96	4.01	-	-
Total	99.29	99.81	100.21	98.83	99.24	99.79	99.73	95.61	96.17	99.13	100.26
Cation/O	5	5	5	5	5	47 (O,OH)	47 (OH, O)	24 (O,OH)	24 (O,OH)	8	8
Si	0.992	0.991	1.008	0.986	0.989	6.849	6.810	5.602	5.621	3.023	2.688
Ti	0.001	0.000	0.001	0.000	0.001	0.277	0.358	0.744	0.665	-	-
Al	2.006	2.005	1.978	2.012	2.008	18.579	18.498	2.834	2.674	1.000	1.333
Mg	-	-	0.000	0.009	-	0.972	1.028	2.779	3.399	0.000	0.000
Ca	-	-	-		-	-	-	0.001	0.000	0.008	0.267
Mn	-	-	0.001	0.000	-	-	-	-		-	-
Fe^{+2}	0.006	0.011	0.012		0.008	2.556	2.585	1.354	1.122	0.000	0.000
Zn	0.000	0.000	0.002	0.002	0.001	0.352	0.305	0.006	0.011	-	-
Na	-	-	-		-	-	-	0.137		0.176	0.709
K	-	-	-		-	-	-	1.699	1.772	0.716	0.008
Total	3.005	3.007	3.002	3.008	3.006	29.584	29.583	15.155	15.263	4.923	5.004

Fig. 5. *Photomicrographs of garnet microporphyroblasts showing microstructural features of inclusion trails, inclusion-matrix relationships, and relict inclusion minerals in group B schists and gneisses. (a) Almost straight inclusion trails mainly of sillimanite and fibrolite oriented oblique to the matrix fabric consisting of quartz, sillimanite, and opaques;* ***XP****; (7). (b) Straight and slightly curved trails of sillimanite and fibrolite in garnet rim oriented parallel to the matrix fabric of coarser sillimanite and quartz;* ***XP****; (7). (c) Garnet core containing straight trails of sillimanite, fibrolite, quartz, and opaques; kyanite (see inset) and staurolite inclusions occur at the outer part of the core; sillimanite inclusion also occurs in the irregular part of the garnet rim;* ***XP****; (10). (d) Garnet core containing two sets of straight inclusion trails; the first set of straight trails at the core consists of fine sillimanite, fibrolite, quartz, spinel and opaques; the second set of trails is oriented at high angle to the first set and is made of coarser sillimanite grains;* ***XP****; (10). (e) Garnet core (right) containing slightly crenulated trails of quartz, graphite, and opaques is surrounded by inclusion free rim with rare fibrolite; Garnet core (left) with weakly oriented fine opaques and a relatively large (1 mm) kyanite inclusion at the mantle area and a few fibrolite grains in the rim; inset shows the kyanite inclusion;* ***XP****; (12). (f) Garnet with two sets of inclusion trails resembling differentiated S1-S2 crenulation cleavages; the trails at the centre are straight but curve slightly at the ends and the second set is oriented at high angle to the first set; both sets are made of biotite, sillimanite, and fibrolite;* ***XP****; (12). (g) Small elongated garnet (1 mm) with straight trails of sillimanite and fibrolite that are parallel to the matrix foliation (Sc);* ***XP****; (12). (h) Fine secondary sillimanite and plagioclase formed at the edge of a garnet;* ***XP****; (10).*

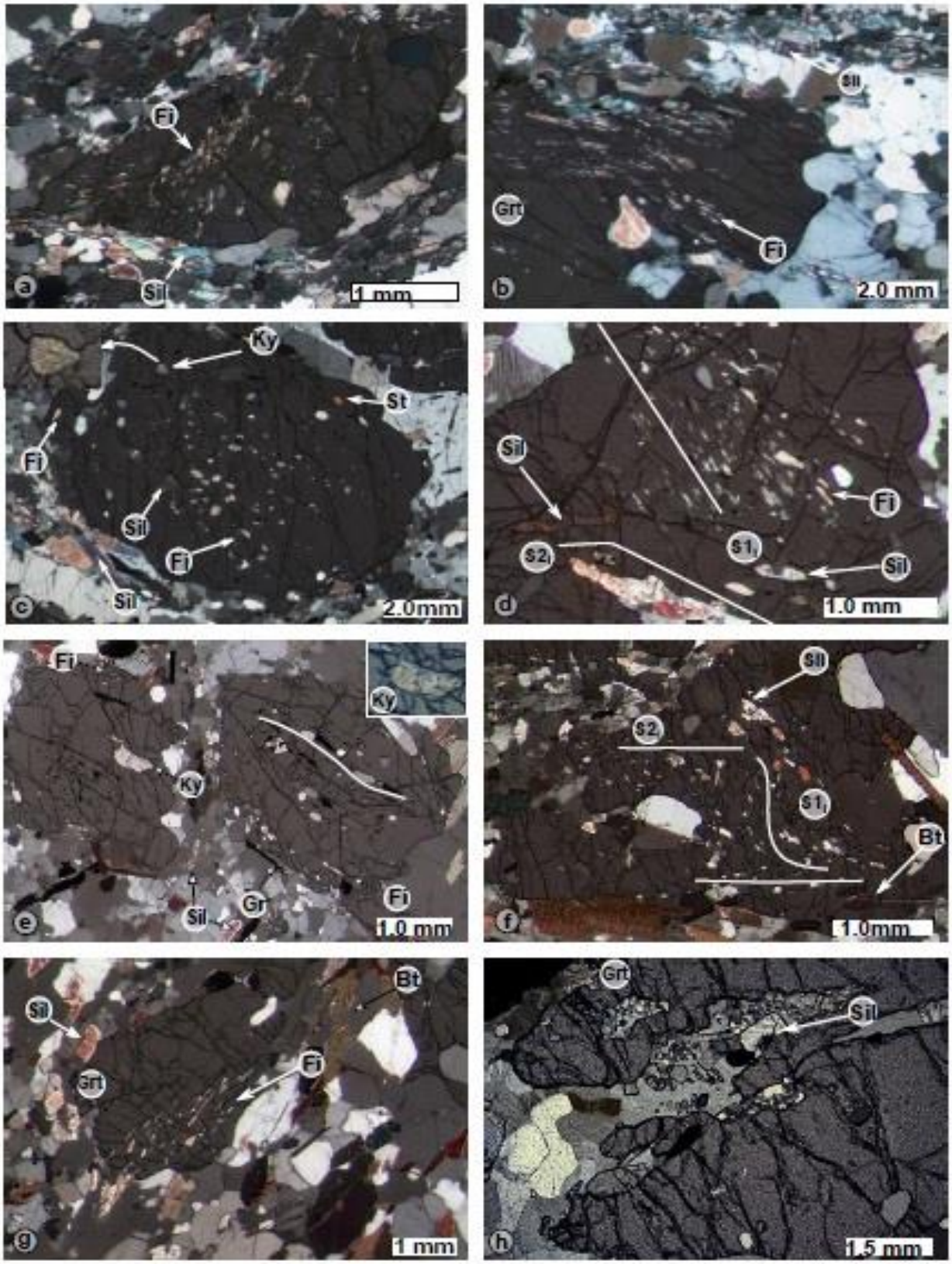
Fi
Sil
1 mm
a
Sil
Grt
Fi
2.0 mm
b
Ky
St
Fi
Sil
Fi
Sil
2.0mm
c
Sil
Fi
S2
S1
Sil
1.0 mm
d
Fi
Ky
Ky
Sil
Gr
Fi
1.0 mm
e
Sil
S2
S1
Bt
1.0mm
f
Bt
Sil
Fi
Grt
1 mm
g
Grt
Sil
1.5 mm
h

Figure 5

Inclusion trails in the porphyroblastic garnets may be straight, gently or strongly crenulated or curved at one end of the trails (Figures 3c-f and 4a). Rarely, inclusion trails define open microfolds and open to tight fold hinges with axial plan fabric (Figure 3g). A few porphyroblasts have straight trails at the centre but turn to opposite directions at the margins (sigmoidal shape) (Figure 3h). The attitude of well-oriented trails in a cluster or adjacent porphyroblasts is diverse and only rarely can the trails be traced from one porphyroblast to another (not through the intervening matrix) (Figure 3d). The trails are commonly oriented oblique to the matrix fabric (Figures 3e-f and 4a). Garnet porphyroblasts in a few samples (e.g. 4) (sample reference no – see Table 1) have straight inclusion trails as the dominant form of inclusion geometry (Figure 3c, d) and these trails consists of quartz, ilmenite, and apatite and in a few instances include staurolite and biotite. The crenulated trails also have similar mineralogy but in places, the quartz inclusions may be larger and longer. Sillimanite and fibrolite are notably absent in the straight or crenulated trails in the cores of garnet porphyroblasts (see below).

Inclusions in some garnet porphyroblasts define two sets of trails that are oriented at high angle to one another (Figure 4f, g). One of them is located in the cores of garnets, it may be straight or crenulated and ends abruptly near the rims, and the other is located near the rim. The grain size of the two sets of inclusions is fine and rather similar. Their geometry resembles part of the differentiated crenulation cleavage commonly seen in low to medium grade rocks but the complete geometry is not recorded any of garnets (see Figure 6b, c of Mathavan and Bowes 2004). Garnet cores in three of the samples (1, 5, 6) have spiral shaped inclusion trails (SSITs) defined mainly by quartz with biotite, staurolite, apatite, and Fe-oxides (Figure 4 c-e). Rare sillimanite occurs in the rims. Garnets in sample 6 show fine smooth SSITs trails at the centre and include coarse quartz grains at the two opposite ends, near the rim (Figure 4d) and garnets in sample 1 appears to have a double spiral trail (Figure 4e).

Inclusions in garnet porphyroblasts define a large inclusion-rich cores surrounded by relatively small inclusion-free rims (Figures 3c-h and 4a-c). Garnet cores host almost all the inclusion minerals listed previously including the relict minerals but the exceptions are sillimanite and fibrolite. These two minerals are notably absent in the large cores of the garnet porphyroblasts in the group A samples but occurrences of sillimanite at the core/mantle area of garnets in a khondalite sample has been reported by Dharmapriya et al. (2017). However, sillimanite, in places as coarse grains, is present in otherwise inclusion-free rims in some garnet porphyroblasts (Figures 3g and 4d). The other minerals that may be present in the inclusion-free part of the rims include opaques, quartz, and K-feldspar. The inclusion-free rim is relatively small (width 1-3 mm) and somewhat irregular but it may represent a large volume of the garnet crystal. In places, coarse matrix minerals protrude into garnet rims and in other places, clusters of sillimanite grains, mostly short prismatic and basal sections embay and partly replace garnet rims. Elsewhere, in places, garnet breaks down at the edges to small sillimanite grains surrounded by plagioclase.

SMALL GARNETS

A minor amount of small (1-2 mm) garnets is usually present in the group A samples, as well as in-group B samples. Often garnets contain straight trails of sillimanite and or fibrolite and in places with quartz and opaques inclusions. The trails are slightly oblique or parallel to the coarser matrix fabric (Figures 4h and 5g).

PORPHYROBLASTIC GARNETS-GROUP B SAMPLES

Porphyroblastic garnets in-group B samples vary in size and shape, nevertheless 3-4 mm subidioblastic to xenoblastic grains are common and some are elongate parallel to the matrix fabric, S_c. Inclusions are abundant in most garnets and as in garnets of group A samples, they often define, a large inclusion-rich cores surrounded by a smaller inclusion-free rims (Figure 5c-d, f). The core-rim relationship is not prominent in some garnets. Sillimanite and fibrolite are the dominant inclusion minerals and the others are quartz, graphite, rutile, ilmenite, spinel, biotite, apatite, corundum, K-feldspar. Relict minerals also occur in a few garnets (see Table 1).

Dimensionally oriented inclusions often define prominent trails. The trail patterns are similar to those of the garnets in-group A samples and the

difference is the dominant presence of sillimanite and fibrolite in the trails. The trails may be straight, gently crenulated, curved, as well as two sets of trails that partly resemble the differentiated crenulation cleavage (Figure 5a-f). The straight trails consisting of sillimanite and fibrolite in some garnets are oriented oblique to the matrix fabric, S_c, defined by sillimanite and quartz (Figure 5a, c). A few larger garnets (6-10 mm) have fewer inclusions in the cores but the rims have straight to slightly curved trails of sillimanite and fibrolite and the trails parallel the matrix fabric (Figure 5b).

Occurrences of relict kyanite inclusions in garnets that have sillimanite and fibrolite-rich cores are significant in-group B samples. A garnet microporphyroblast in sample 10 has a large inclusion-rich core defined mainly by dimensionally oriented sillimanite, fibrolite, quartz, and opaques. Staurolite and kyanite occur in the mantle area of the garnet and sillimanite occurs again in the outer rim (Figure 5c). Thus, the sequence of the inclusion minerals from the core to rim is sillimanite-kyanite-sillimanite. Raase and Schenk (1994, see their Figure 3a, b) first reported this inclusion sequence in a metapelite sample from the eastern HC. Kyanite inclusions occur in the mantle area of a garnet microporphyroblast in another sample (12) and fibrolite occurs at the rim of the garnet (Figure 5e). The other garnets in the sample have sillimanite in the cores.

MICROSTRUCTURAL FEATURES-INTERPRETATION

GARNET PORPHYROBLASTS-GROUP A SAMPLES

Growth of garnet porphyroblasts has taken place after the development of straight inclusions trails preserved within the garnet cores (Figures 3b-d and 4a). These trails represent the earliest recognisable planner fabric, S1, produced by D1 deformation and the garnet cores have overgrown this fabric during early D2 deformation (see Mathavan and Bowes, 2004, 2005). Quartz and ilmenite mainly makeup $S1_i$ (i - internal) fabric, apatite and rutile contribute in places and to a lesser extent, biotite and staurolite.

Muscovite is a major constituent of high-grade pelitic staurolite schists in many regions (e.g. Eastern Grampians, Scotland – McLellan, 1985) and thus it would have been part of early S1, but completely consumed by the garnet forming reaction subsequently (see below). However, sillimanite and fibrolite were not part of this S1, as they do not occur in the cores of garnet porphyroblasts in the schists. Likewise, kyanite (+ hercynite) is not part of S1, as they are the product of the reaction that formed the cores of garnet porphyroblasts (see later). Thus, the precursor rock/s to the schists would have been high-grade staurolite schists with quartz, muscovite, biotite, and staurolite as major constituents and chlorite and garnet might have been additional constituents.

The different shapes and forms of the curved and crenulated trails preserved within the garnet cores (Figure 3 e-h) are interpreted as representing stages 2 and 3 crenulation cleavage development of Bell and Rubenach (1983) and the host porphyroblasts are inferred to have overprinted them during early phases of D2 deformation.

The grain size of minerals that makeup the two sets of inclusion trails present in the cores of some garnets is not significantly different (Figure 4f, g) but the grains are much smaller than the matrix minerals (Figure 5d, f). Thus, the timing of growth of minerals that form the second set of inclusion is constrained by the timing of the major coarsening of the matrix minerals in the schists and gneisses as well as the significant grain coarsening in the HC (see Voll and Kleinschrodt, 1991). According Berger and Jayasinghe (1976), the major F3 folds refolded the compositional layering without significant reconstitution and development of an axial planar fabric and Yoshida et al. (1990) reported faint development of schistosity (foliation) along the axial surfaces and strong biotite schistosity parallel to banding of D3 folds. Thus, it is most likely that the major grain coarsening in the HC rocks would have been associated with late-to post-D2 deformation phase, predating D3 folds of Berger and Jayasinghe (1976) and coeval with the peak granulite metamorphism in the HC. Kehelpannala (1997) inferred that the peak granulite metamorphism was coeval with D2 and D3 phases of deformation. Accordingly, the minerals that constitute the second set of inclusion trails are interpreted to have grown during the development of S1-S2 differentiated crenulation cleavage early in D2 and the garnets have over printed this fabric subsequently. The

major coarsening of matrix was in late- to post-D2 deformation.

In contrast, the porphyroblast growth model of Bell and Hayward (1991) suggests that porphyroblast or its rims do not or cannot overgrow a differentiated crenulation cleavage during the same deformation that produced the cleavage but do so during the subsequent deformation. Moreover, Bell and Hickey (1999) and Johnson (1999) concluded that either porphyroblasts with two sets of orthogonal inclusion trails grow during successive phases of deformation or helicitically overgrow the differentiated crenulation during a subsequent deformation. However, the metamorphic deformation model of Williams (1984) for microstructure development in first cycle immature arc related sediments, accounts for growth of porphyroblasts containing S1-S2 inclusion geometries during the same phase of deformation that produced the cleavage. The model suggests that chlorite consuming reactions lead to pulses in the rates of fabric evolution and the consumption of chlorite over a narrow temperature range result in a reaction softening effect and the fabric evolves rapidly initially. Once the rate of water production diminished with the cessation of chlorite consuming reactions, the transition to homogeneous fabric (S2) occurs at diminishing rate and the porphyroblasts are able to overgrow S1-S2 crenulation cleavages. Consumption of muscovite and staurolite (see later) would have had somewhat similar effects on the rate of fabric evolution in the schists and gneisses enabling the garnet porphyroblasts to overgrow S1-S2 crenulation cleavage during early D2.

Garnets with spiral shaped inclusion trails are traditionally interpreted in terms of syn-tectonic growth during non-coaxial deformation (Spry, 1963; Rosenfeld, 1970; Schoneveld, 1977; Passchier et al., 1992 and others). This model envisages continued growth and rotation of porphyroblasts in response to non-coaxial deformation, simultaneously incorporating adjacent matrix minerals as spiral shaped trails. The presence of coarse quartz grains on opposite sides of the smoothly curving trails as noted in the porphyroblast garnet (Figure 4d) probably represent quartz grains from an earlier pressure shadow that have subsequently been incorporated in the growing garnet porphyroblast. Thus, these garnets may have formed in manner envisaged in the traditional syn-tectonic growth model. Garnet cores with SSITs may have formed at localities where the conditions were conducive for nucleation and growth of garnet porphyroblasts and D2 deformation had a strong non-coaxial component. Presence of rare relict staurolite inclusion probably establishes that the garnet growth is linked to D2 deformation.

The small garnets in the schists containing straight trails of small sillimanite and fibrolite that are parallel or slightly oblique to the matrix fabric (Figure 4h) have grown during late- to post-D2 deformation when sillimanite and fibrolite were fabric-forming minerals.

Absence of reference mineral growth precludes establishing firmly the timing of development of the inclusion free rims of the garnet porphyroblasts. However, the presence of rare coarse sillimanite inclusion in the rims (Figure 3g) suggests that this growth was at least late in D2, at the same time as the growth of the small garnets containing sillimanite and fibrolite inclusion trails that are parallel to the matrix fabric and the coarsening of matrix. That the rims are mostly inclusion free may be due to slower growth rate and or elevated temperatures that allowed enhanced diffusion of potential inclusion components away from growing garnet (Spry, 1969; Williams, 1984; Mathavan and Bowes, 2004).

The growth of large inclusion-rich garnets cores early in D2 deformation was in the kyanite stability field as kyanite is a part of the core inclusions, in places being part of deformed S1. In other instances, it occurs as non-oriented inclusion. Presence of rare sillimanite inclusions indicate that sillimanite field condition prevailed during the growth of garnet rims.

GARNET MICROPORPHYROBLASTS-GROUP B SCHISTS AND GNEISSES

Microstructural evidence indicates that growth of garnet cores in-group B samples has taken place early in D2 as in-group A samples, after the development of straight inclusion trails. However, the garnet cores have overprinted straight trails of sillimanite and fibrolite and thus the growth was in the sillimanite stability field (Figure 5a, c). Garnet cores containing gently curved trails (Figure 5e) and two sets of trails (Figure 5d, f) suggest that garnet continued to grow as the matrix fabric deformed

and evolved to form the S1-S2 differentiated cleavage.

Presence of kyanite inclusions in the mantle area and sillimanite in the rim of garnets indicate that the PT conditions changed to that of the kyanite stability field during the growth of mantle area, followed by growth of the rims in the sillimanite stability field. The growth of garnet rims was in late- to post-D2 deformation time, evident from that sillimanite and fibrolite trails in some garnet rims parallel or slightly oblique to the matrix fabric (Figure 5b).

The elongate garnets and the small garnets, some of them having sillimanite trails parallel to matrix also must have grown during late- to post-D2 deformation.

MINERAL REACTIONS

GROUP A SAMPLES

The presence of relict kyanite, staurolite, and biotite inclusions in the cores of garnets indicates that the breakdown of staurolite led to the growth of cores of the garnet porphyroblasts and kyanite by reaction 1, as in the kyanite-sillimanite zone of the Scottish Dalradian (e.g. Farber et al., 2014) and also see Dharmapriya et al. (2017) (Abbreviations follow Kretz, 1983).

$$Ms + St + Qtz = Grt + Ky + Bt + H_2O \quad (1)$$

Upon further heating and increase in temperature in late D2, sillimanite was produced (reaction 2), instead of kyanite, coupled with growth of inclusion-free rims of the garnet porphyroblasts. Sillimanite became part of the matrix that earlier had kyanite and rarely included in the garnet rims.

$$Ms + St + Qtz = Grt + Sil + Bt + H_2O \quad (2)$$

Growth of garnet rims would have ceased with the complete consumption of staurolite but muscovite may have persisted, as it is present in sillimanite zone rocks in other regions (e.g. Scottish Dalradian- McLellan, 1985). However, the complete disappearance of biotite and muscovite in the matrix is probably due to progression of the terminal reactions 3 and 4.

$$Ms + Qtz = Sil + Kfs + H_2O \quad (3)$$

$$Bt + Qtz + Sil = Grt + Kfs + H_2O \quad (4)$$

Absence of kyanite in the matrix suggests that reaction 2 accompanied the transformation of kyanite to sillimanite via reaction 5, and this transformation is consistent with the microstructural evidence for direct replacement of kyanite by sillimanite in a khondalite sample reported by Dharmapriya et al. (2017). In addition, somewhat prismatic shaped clusters of sillimanite grains observed at the rims of garnets and in the matrix of some schist likely represent pseudomorphed kyanite (cf. Raase and Schenk, 1994).

$$Ky = Sil \quad (5)$$

Reaction 4 may have formed the small garnets in the sillimanite- and fibrolite- bearing matrix and the local assemblages within the garnets such as kyanite-hercynite and kyanite-corundum may be as a result of reactions 6 and 7, as suggested by Hiroi et al. (1994).

$$St = Ky + Hc + Grt + H_2O \quad (6)$$

$$St = Ky + Crn + Grt + H_2O \quad (7)$$

GROUP B SAMPLES

Some garnets in-group B schists preserve S1 fabric as straight trails defined by sillimanite, fibrolite, and quartz, indicating that sillimanite developed early in the host rocks during D1 deformation. Lack of microstructural and mineralogical evidence hinders determining the prograde reaction that produced the early D1 sillimanite and fibrolite. The study by McLellan (1985) suggests that during the progressive Barrovian type of metamorphism of pelites, bulk rock Mg / (Mg + Fe) content controls the breakdown of staurolite and it breaks down early in relatively magnesian rocks producing kyanite rather than sillimanite. Thus, though the group B schists are relatively magnesian compared to the group A khondalites (see later), it is unlikely that staurolite was involved in the growth of early sillimanite in these rocks and the other likely candidates are reaction 8 or 9 (Zhao and Cawood, 1999).

Presence of chlorite in pelitic staurolite schists depends largely on the reaction/s that produces staurolite (e.g. see reactions 2 and 3 of Farber et al. (2014). Magnesian nature of group B samples suggests that chlorite might have present earlier in the rocks. If chlorite were present earlier in the group B schists, then the

reaction 8 would have produced the early D1 sillimanite and consumed chlorite completely. In the absence of chlorite in D1 matrix, reaction 9 would be more likely candidate that produced D1 sillimanite.

$$Chl + Ms = Bt + Sil + Qtz + H_2O \quad (8)$$

$$Grt + Ms = Sil + Bt + Qtz \quad (9)$$

Occurrence of rare relict staurolite inclusions in the porphyroblastic garnets of group B samples suggest that breakdown of staurolite may have been responsible for growth of these garnets as in the group A samples. However, the reactions appear to have progressed in the reverse order in-group B samples. Reaction 2 may have been responsible for the growth of garnet cores that overprinted the matrix fabric containing sillimanite and fibrolite. Garnets continued grow but now under kyanite stability conditions, possibly due to the progression of reaction 1, and enclosed kyanite and staurolite as inclusions within garnets (Figure 5c and e). Late in D2, when sillimanite stability conditions were re-established, the rims of garnet and the small garnets containing sillimanite trails that are parallel to the matrix fabric formed by reactions 2 and 4 respectively. Reaction 4 may have not gone to completion in some samples because of deficiency of sillimanite, and biotite remains in the matrix (see Raase and Schenk, 1994).

MINERAL COMPOSITION

Mineral analyses were performed on the Cameca-Camebax microprobe at the Department of Geology (now School of Earth Sciences), University of Glasgow and the operating conditions were 20 kV and 20 nA beam current. An online ZAF correction procedure was used for all data reduction and Tables 2 and 3 show selected analyses of minerals in the samples studied.

Garnet: The garnets are essentially almandine-pyrope solid solutions but the garnets in the group A samples, particularly in khondalites, are relatively richer in almandine (82-66% almandine, 13-27 % pyrope) compared to those in the other schists (73-56% almandine, 37-24% pyrope) (Table 2). As the garnet is the sole Fe-Mg mineral in the schists (biotite is present in the gneisses), apart from minor amounts of relict inclusions of staurolite and biotite, the Mg/(Mg + Fe) ratios of the garnets reflect the bulk Mg/(Mg + Fe) ratios of the host schists. The khondalites are therefore poorer in magnesium than the other schists (Table 2). Microprobe traverses across core-rim textural zonation, in a number of garnets indicate that they are generally homogeneous in composition with the exceptions of minor variation shown in a few garnets near the rims where CaO content decreases slightly with the corresponding increase in either MgO or FeO.

Staurolite: The relict staurolite grains have compositions similar to those reported by Hiroi et al. (1984) with high Al_2O_3 (57-56%) and TiO_2 (1.50-1.34%) and low SiO_2 (24%) and these chemical features are considered as characteristics of granulite facies rather than amphibolite facies staurolite (e.g. Hiroi et al. 1984). ZnO content of the staurolites ranges between 1.7 and 1.2% (Table 3).

Aluminosilicates: The kyanite and sillimanite inclusions in garnets as well as the matrix sillimanite have virtually pure compositions and the amount of TiO_2 and FeO is less than 0.5 % (Table 3).

Biotite: Biotite inclusions in garnet are relatively rich in TiO_2.

DISCUSSION

Group A schists (including khondalites) have a two-stage growth history with their inclusion-rich cores preserving information about the early stages of deformation and metamorphism. Their inclusion-free rims together with minerals in the matrix provide evidence for development at later stages of metamorphism. Microstructural evidence indicates that the growth of cores of the garnet porphyroblasts coincides with the development of a crenulation cleavage formed during D2 deformation. A two-stage growth history for garnets in the metapelites from the Wanni Complex has been suggested previously (Kehelpannala, 1997, 2003) though the metamorphic conditions during garnet growth were not well constrained, in part because relict kyanite and staurolite inclusions have not been found so far in the Wanni Complex rocks.

The two-stage growth history of porphyroblastic garnets reflects the prograde *P-T-t* path undergone by the HC rocks (see Figure 2). The

growth of large garnet cores was in the kyanite field before kyanite gave way to sillimanite during the growth of garnet rims. The steep pressure gradient of the early prograde path and the growth of large garnet cores suggest sustained deep burial and crustal thickening. The early crustal thickening would have resulted in considerable flattening and stretching during D1 as evident in the straight quartz inclusion trails in some of the garnet porphyroblasts (e.g. Figure 3c). Furthermore, tectonic events associated with continent-continent type collisions (Dharmapriya et al., 2017) or magmatic arc related collisions (Santosh et al., 2014; He et al., 2016) during the assembly of Gondwana would have caused further crustal thickening. This collisional environment would have setup initially compressional stress regimes favourable for the development of crenulation cleavage early in D2 and predominantly non-coaxial deformational conditions subsequently.

The growth history of garnets in the group B samples spans the sillimanite-kyanite-sillimanite stability fields and reflects the extended prograde segment of the *P-T-t* path (see Figure 2). In addition, microstructural and inclusion mineral evidence indicate that sillimanite stability field conditions prevailed during D1 and in early D2 deformation during the growth of large inclusion-rich garnet cores.

The mineralogy of the S1 fabric preserved as straight trails within the cores of garnet porphyroblasts in-group A samples is mainly quartz, ilmenite, rutile and biotite (+ staurolite) and thus indicates staurolite zone (amphibolite facies) metamorphic condition during D1. Kyanite formed early in D2 and sillimanite was not formed until later in these rocks. In contrast, garnets in group-B samples have sillimanite and fibrolite as the prominent constituents of S1i fabric and thus pointing to sillimanite zone (amphibolite facies) condition during D1. Thus, evidently early sillimanite and fibrolite were formed during D1 deformation in-group B schists and gneisses but later, during late- to post-D2 phase deformation in-group A schists. Consequently, the metamorphic grade (temperature) appears to have developed asynchronously across the Highland Complex during D1 deformation. Further microstructural study is required to confirm the above inference that sillimanite formed early in some localities with respect to D1. However, if it is confirmed, it has implications for tectonothermal models and suggests availability of additional heat source/s in certain areas/regions of the HC. The convergent magmatic arc model proposed by Santosh et al. (2014) and He et al. (2016) provides a tectonic environment for additional heat sources in the form of magmatic activity and or related fluids.

It is not understood well why the group A schists have not recorded the mineral inclusion evidence for the lower part of the prograde *P-T* segment, going from sillimanite to kyanite stability fields (see Figure 2). Large thin sections (6 x 4.5 cm) have been used to study the khondalite samples and therefore it is unlikely that slicing of thin sections would have possibly masked the presences of sillimanite inclusions pre-dating kyanite inclusions in the garnets. As noted previously, the thermobarometry data indicate that the combined HC and WC unit represents a more or less continuous but tilted section of the lower crust. Thus, it unlikely that the two groups of samples, A and B, would have come from two different crustal levels. Perhaps, conditions that were favourable to form early S1 sillimanite not existed for the group A samples and therefor sillimanite did not form early. Thus, garnets in-group A schists did not and were not able to enclose sillimanite inclusions pre-dating kyanite inclusions.

The straight trails of sillimanite, fibrolite, quartz and opaques present in the small garnets, both in-group A and B schists, parallel or slightly oblique to the coarser matrix fabric (S_c) and thus these trails represent lately formed matrix fabric rather than early S1. Moreover, there was no sillimanite or fibrolite in the S1 matrix in-group A schists. These small garnets have single stage growth history.

Garnets in both groups of schists are chemically unzoned across the texturally zoned inclusion-rich cores and inclusion-free rims. The absence of chemical zoning across the garnets indicates re-equilibration and chemical homogenization due to volume diffusion during the high-grade metamorphism that lasted long (see below) (e.g. Blackburn, 1969; Fernando et al., 2003).

Nucleation of garnet began during the early phase of D2 deformation coinciding with the initial development of the crenulations that possibly created favourable sites, such as crenulations hinges, for nucleation and growth

of porphyroblastic garnets (e.g. Bell et al., 1986). Microstructural evidence indicates that nucleation was progressive and once nucleated, the growth was relatively rapid (cf. Spry, 1969; Vernon, 1976; Williams, 1984; Mathavan and Bowes, 2004) and that enabled the growing garnet cores to incorporate the reactant mineral (e.g. staurolite) and the product mineral (e.g. kyanite) as well as parts of the matrix fabric present at that time. The rapid growth also enabled garnet cores to overprint the evolving matrix fabric resulting in some cases, presence of garnets with different inclusion geometries, including garnets with straight, gently crenulated, and S1-S2 trails in the same sample (Figures 3e and 5e, f) (e.g. Johnson, 1999). The microstructural evidence also suggests temporal coincidence of nucleation and growth garnet porphyroblasts and the progression of the prograde reactions.

The principal mechanism of porphyroblast growth involves progressive outward growth by chemical replacement involving grain-scale diffusion (e.g. Passchier and Trouw, 2005). The outward growth enables garnet porphyroblasts to enclose and preserve from the core to rim a sequence of minerals formed at different PT conditions and thus preserve information about the evolving *P-T-t* path. The rare occurrence of the sequence of sillimanite – kyanite – sillimanite inclusions from the core to rim in one of the garnets in group B samples, and the same sequence reported by Raase and Schenk (1994) are examples where the information about the extended part of the evolving PT conditions are preserved in a single porphyroblastic garnet.

S1 fabric is absent in the present matrix that hosts the garnets in the studied samples. Microstructural evidence indicates that S1 preserved as straight trails within the cores of garnet porphyroblasts was deformed, crenulated, and transposed to form the S2i fabric that led to the development of the present matrix. Thus, the present schistose foliation is a composite foliation (S_c), formed from transposed S1, newly formed S2 and possibly includes S0 (see Kröner et al., 1994b). Thus, reorientation and transposition of earlier fabrics, which had considerable amounts of biotite and muscovite in the matrix originally, has largely determined the discordance between inclusion trails and the external matrix fabric with the exception being the garnet cores containing SSITs. The growth of SSITs garnets is envisaged in terms of classical syn-tectonic rotational growth during non-coaxial deformation (Spry, 1963; Rosenfeld, 1970; Schoneveld, 1977; Passchier et al., 1992). Field evidence for non-coaxial deformation has been recorded at several localities in the HC (e.g. Kröner et al., 1994b) and thus it would have played a role in the growth of SSITs garnets.

Contrasting sizes of the inclusion minerals and the corresponding matrix minerals, particularly quartz and sillimanite, indicate significant coarsening of the matrix following the growth of porphyroblastic garnets. Kriegsman (1991) estimated the size difference of sillimanite in some khondalites is of the order 1:10-50 (inclusion: matrix). The coarsening resulted from collective recrystallization, driven by grain boundary free energy while the peak metamorphic temperature (>850°C) was maintained over a considerable period. The zircon U–Pb geochronology study by He et al. (2018) on the mafic granulites of the HC, gives insight into the time span involved during the coarsening. Their study indicates the high temperature metamorphism of the HC was long lasting, of the order of 100 Ma, and they suggested that substantially elevated rates of crustal heat production sustained the high temperature over that period. The pronounced annealing has locally produced granoblastic matrix grains in the schists but has not completely outlasted the strong effects of D2 deformation and dimensionally aligned elongate and ribbon quartz and long prismatic sillimanite grains persist in the matrix.

Microstructural evidence of melting is lacking in the studied schists, although the peak metamorphic temperature was over 850°C (see Hiroi et al., 1997). The prograde reactions are considered as dehydration reactions rather than dehydration melting reactions. Dharmapriya et al. (2017), however, inferred partial melting during peak metamorphism in their studied khondalite samples. Raase and Schenk (1994) observed that partial melting was not extensive in the HC and the leucosomes are not volumetrically abundant. This may be due either to the granulites been dehydrated at high temperature or activity of H_2O was reduced due to the presence of CO_2 and other fluids (see Raase and Schenk, 1994). The euhedral plagioclase inclusions found in some garnet rims (e.g. in sample 4) could possibly be

interpreted as evidence for melting (cf. Hiroi et al., 1995) but they have corroded quartz within them, indicating these plagioclase grains were formed due to instability between the host garnet and the quartz inclusions and not the product of crystallization from melt. None of the matrix K-feldspar grains shows euhedral shape and the quartz-K-feldspar clusters show granoblastic grain boundaries reflecting prolonged annealing. Development of K-feldspar crystal faces on the quartz grains would have indicated crystallization from melt (cf. Vernon and Collins, 1988; Vernon, 2011).

CONCLUSIONS

Garnet porphyroblasts in the metapelites of the HC have a multiple growth history. They grew during a D2 phase of deformation corresponding with the development of crenulation cleavage and their growth history reflects the prograde *P-T-t* path undergone by the HC.

Microstructural evidence for the development of crenulation cleavage is preserved exclusively within the cores of porphyroblastic garnet in the form of inclusion trails with either straight, crenulated geometries, or grains that possess two sets of trails. Collectively these inclusion trails are the expression of a progressively developed crenulation cleavage, S1-S2.

Porphyroblastic garnets in a group of metapelites that include the khondalites (group A schists) have a two-stage growth history. Their large inclusion-rich cores formed in an early D2 phase of deformation under kyanite field stability. The inclusion-free rims grew on the cores in a late- to post-D2 phase of deformation under sillimanite field stability.

Porphyroblastic garnets in another group of metapelites (group B schists) have a more protracted growth history. Their inclusion-filled cores grew early in D2 phase of deformation under sillimanite field stability, followed by growth of the outer part of cores under kyanite field stability and the inclusion-free rims grew during late- to post D2 phase of deformation under sillimanite field stability. Nucleation of garnet was progressive and the growth was relatively rapid. That enabled garnets to enclose and preserve the reactant mineral/s and the product mineral/s and parts of the evolving matrix fabric elements. The outward growth enabled garnets to preserve a sequence of minerals formed at different PT conditions from its core to rim.

A major grain coarsening that followed the growth of garnet porphyroblasts during the peak granulite metamorphism established the characteristic of the matrix that hosts the garnets. This matrix did not completely outlast the effects of intense D2 deformation. The U–Pb geochronology study of He et al. (2018) indicates that this period of annealing may be long, of the order 100 Ma.

The metamorphic grade (temperature) prevailing during D1 deformation appears to be asynchronous across the HC: in some rocks, staurolite zone condition prevailed whereas in others metapelites, sillimanite zone temperature prevailed, indicating contributions from additional heat source/s I some localities/regions.

ACKNOWLEDGEMENTS

The manuscript benefitted from critical comments and suggestions on the first version by Nick Mortimer/GNS. The author gratefully acknowledges the careful and constructive review of the manuscript by Alan Cooper/ Geology Otago. Grateful acknowledgement is made to Mark Lawrence/GNS Avalon for providing microphotography facilities. Acknowledgement is also made of an EU Marie Curie Fellowship and the facilities provided at the University of Glasgow. The author appreciates the anonymous referee's useful suggestions and comments.

REFERENCES

Almond, D.C. (1994) Solid rock geology of the Kandy area, Sri Lanka. Institute of Fundamental Studies, Hantana road, Kandy, Sri Lanka.

Baba, S. (1998) Proterozoic anticlockwise *P-T* path of the Lewisian Complex of South Harris, Outer Hebrides, NW Scotland. Journal of Metamorphic Geology, 16: 819–841.

Bell, T.H. and Rubenach, M.J. (1983) Sequential porphyroblast growth and crenulation cleavage development during progressive deformation. Tectonophysics, 92: 171–194.

Bell, T.H., Rubenach, M.J. and Fleming, P.D. (1986) Porphyroblast nucleation, growth and dissolution in regional metamorphic rocks as a function of deformation partitioning during foliation development. Journal of Metamorphic Geology, 4: 37–67.

Bell, T.H. and Hayward, N. (1991) Episodic metamorphic reactions during orogenesis: the control of deformation partitioning on reaction sites and reaction duration. Journal of Metamorphic Geology, 9 : 619–640.

Bell, T.H. and Hickey, K.A. (1999) Complex microstructures preserved in rocks with a simple matrix: Significance for deformation and metamorphic processes. Journal of Metamorphic Geology, 17: 521–535.

Berger, A.R. and Jayasinghe, N.R. (1976) Precambrian structure and chronology in the Highland Series of Sri Lanka. Precambrian Research, 3: 559–576.

Blackburn, W.H. (1969) Zoned and unzoned garnets from the Grenville gneisses around Gananoque, Ontario. Canadian Mineralogist, 9: 691–698.

Cooray, P.G. (1962) Charnockites and their associated gneisses in the Precambrian of Ceylon. Quarterly journal of the Geological Society of London, 118: 239–273.

Cooray, P.G. (1984) An Introduction to The Geology of Sri Lanka, Second. ed. National Museums of Sri Lanka Publication.

Cooray, P.G. (1994) The precambrian of Sri Lanka: a historical review. Precambrian Research, 66: 3–18.

Dharmapriya, P.L., Malaviarachchi, S.P.K., Santosh, M., Tang, L. and Sajeeve, K. (2015) Late-Neoproterozoic ultrahigh-temperature metamorphism in the Highland Complex, Sri Lanka. Precambrian Research, 271: 311–333.

Dharmapriya, P.L., Malaviarachchi, S.P.K., Sajeev, K. and Zhang, C. (2016) New LA-ICPMS U–Pb ages of detrital zircons from the Highland Complex: insights into late Cryogenian to early Cambrian (ca. 665–535 Ma) linkage between Sri Lanka and India. International Geology Review, 58: 1856–1883.

Dharmapriya, P.L., Malaviarachchi, S.P.K., Kriegsman, L.M., Galli, A., Sajeev, K. and Zhang, C. (2017) New constraints on the P–T path of HT/UHT metapelites from the Highland Complex of Sri Lanka. Geoscience Frontiers, 8: 1405–1430.

Farber, K., Caddick, M.J. and John, T. (2014) Controls on solid-phase inclusion during porphyroblast growth: insights from the Barrovian sequence (Scottish Dalradian). Contributions to Mineralogy and Petrology, 168: 1–17.

Faulhaber, S. and Raith, M. (1991) Geothermometry and Geobarometry of High-Grade Rocks: A Case Study on Garnet-Pyroxene Granulites in Southern Sri Lanka. Mineralogical Magazine, 55: 33–56.

Fernando, G.W.A.R., Hauzenberger, C.A., Baumgartner, L.P. and Hofmeister, W. (2003) Modeling of retrograde diffusion zoning in garnet: evidence for slow cooling of granulites from the Highland Complex of Sri Lanka. Mineralogy and Petrology, 78: 53–71.

He, X.F., Santosh, M., Tsunogae, T., Malaviarachchi, S.P.K. and Dharmapriya, P.L. (2016) Neoproterozoic arc accretion along the 'eastern suture' in Sri Lanka during Gondwana assembly. Precambrian Research, 279: 57–80.

He, X.F., Hand, M., Santosh, M., Kelsey, D.E., Morrissey, L.J. and Tsunogae,T. (2018) Long-lived metamorphic P–T–t evolution of the Highland Complex, Sri Lanka: Insights from mafic granulites. Precambrian Research, 316: 227–243.

Hiroi, Y., Yoshida, M. and Vitanage, P.W. (1987) Relict kyanite in the Highland and Southwest gneisses in Sri Lanka: evidence of prograde metamorphism and characteristics in common with the Lützow-Holm Complex in East Antarctica, in: Jayawardena, D.E de S., Cooray, P.G., and Dahanayake, K. (Ed.), Precambrian Events in the Gondwana Fragments. Geological Society of Sri Lanka, Special Publication 3, p. 28.

Hiroi, Y., Ogo, Y. and Namba, K. (1994) Evidence for prograde metamorphic evolution of Sri Lankan pelitic granulites, and implications for the development of continental crust. Precambrian Research, 66: 245–263.

Hiroi, Y., Motoyoshi, Y., Shiraishi, K. and Ellis, D.J. (1995) The significance of euhedral calcic plagioclase inclusions in garnet from the Lützow-Holm complex, east Antarctica: a textural indicator of partial melting in pelitic gneisses, in: Proceedings of the NIPR Symposium on

Antarctic Geosciences, No 8, National Institute of Polar Research, Tokyo. pp. 107–120.

Hiroi, Y., Motoyoshi, Y., Shiraishi, K. and Mathavan, V. (1997) Local formation of hercynite-plagioclase symplecitite after garnet and sillimanite in khondalite from Habarana, Sri Lanka: mineral textures, in: Proceedings of the NIPR Symposium on Antarctic Geosciences, No 10, National Institute of Polar Research, Tokyo. pp 153–164.

Hölzl, S., Köhler, H., Kröner, A., Jaeckel, P. and Liew, T.C. (1991) Geochronology of the Sri Lankan basement, in: The Crystalline Crust of Sri Lanka, Part I. Summary of Research of the German-Sri Lankan Consortium. Kröner, A. (Ed.), Professional Paper 5, Geological Survey Department, Sri Lanka, pp. 237–257.

Hölzl, S., Hofmann, A.W., Todt, W. and Köhler, H. (1994) U-Pb geochronology of the Sri Lankan basement. Precambrian Research, 66: 123–149.

Johnson, S.E. (1999) Porphyroblast microstructures: a review of current and future trends. American Mineralogist, 84: 1711–1726.

Johnson, S.E., Dupee, M.E. and Guidotti, C. V. (2006) Porphyroblast rotation during crenulation cleavage development: An example from the aureole of the Mooselookmeguntic pluton, Maine, USA. Journal of Metamorphic Geology, 24: 55–73.

Kehelpannala, K.V.W. (1997) Deformation of a High-Grade Gondwana Fragment, Sri Lanka. Gondwana Research, 1: 47–68.

Kehelpannala, K.V.W. (2003) Structural evolution of the middle to lower crust in Sri Lanka- a review. Journal of Geological Soceity of Sri Lanka, 11: 45–85.

Kehelpannala, K.V.W. (2004). Arc accretion around Sri Lanka during the assembly of Gondwana. Gondwana Research 7: 1323–1328.

Kim, Y., Cho, M. (2008) Two-stage growth of porphyroblastic biotite and garnet in the Barrovian metapelites of the Imjingang belt, central Korea. Journal of Metamorphic Geology, 26: 385–399.

Kleinschrodt, R.(1994) Large-scale thrusting in the lower crustal basement of Sri Lanka. Precambrian Research, 66: 39–57.

Kretz, R. (1983). Symbols for rock-forming minerals. American Mineralogist, 68: 277–279.

Kriegsman, L.M. (1991) Structural geology of the Sri Lankan basement – a preliminary review, in: The Crystalline Crust of Sri Lanka, Part I, Summary of Research of the German-Sri Lankan Consortium. Kröner, A. (Ed.), Professional Paper 5, Geological Survey Department, Sri Lanka, pp. 52–68.

Kriegsman, L.M. and Schumacher, J.C. (1999) Petrology of Sapphirine-bearing and associated granulites from central Sri Lanka. Journal of Petrology, 40: 1211–1239.

Kröner, A., Jaeckel, P. and Williams, I.S. (1994a) Pb-loss patterns in zircons from a high-grade metamorphic terrain as revealed by different dating methods: U-Pb and Pb-Pb ages for igneous and metamorphic zircons from northern Sri Lanka. Precambrian Research, 66: 151–181.

Kröner, A., Kehelpannala, K.V.W. and Kriegsman, L.M. (1994b) Origin of compositional layering and mechanism of crustal thickening in the high-grade gneiss terrain of Sri Lanka. Precambrian Research, 66: 21–37.

Kröner, A., Rojas-Agramonte, Y., Kehelpannala, K.V.W., Zack, T., Hegner, E., Geng, H.Y., Wong, J. and Barth, M. (2013) Age, Nd-Hf isotopes, and geochemistry of the Vijayan Complex of eastern and southern Sri Lanka: A Grenville-age magmatic arc of unknown derivation. Precambrian Research, 234: 288–321.

Mathavan, V., Prame, W.K.B.N. and Cooray, P.G. (1999). Geology of the High Grade Proterozoic Terrains of Sri Lanka, and the Assembly of Gondwana: an Update on Recent Developments. Gondwana Research, 2, 237–250.

Mathavan, V. and Bowes, D.R. (2004). Microstructural features of albite porphyroblasts as indicators of sequential Barrovian metamorphic mineral growth in the Caledonides of the SW Scottish Highlands. Journal of Metamorphic Geology, 22: 639–651.

Mathavan, V. and Bowes, D.R. (2005). Multiple growth history of porphyroblasts in Barrovian metamorphism of Dalradian albite schists near Loch Lomond, SW Scottish Highlands. Scottish Journal of Geology, 41: 175–188.

McLellan, E. (1985) Metamorphic reactions in the kyanite and sillimanite zones of the

barrovian type area. Journal of Petrology, 26:789–818.

Milisenda, C.C.., Liew, T.C.., Hofmann, A.W. and Kröner, A. (1988) Isotopic Mapping of Age Provinces in Precambrian High-Grade Terrains: Sri Lanka. The Journal of Geology, 96: 608–615.

Milisenda, C.C., Liew, T.C., Hofmann, A.W. and Köhler, H. (1994) Nd isotopic mapping of the Sri Lanka basement: update, and additional constraints from Sr isotopes. Precambrian Research 66: 95–110.

Osanai, Y., Sajeev, K., Owada, M., Kehelpannala, K.V.W., Prame, W.K.B.N., Nakano, N. and Jayatilek, S. (2006) Metamorphic evolution of high-pressure and ultrahigh-temperature granulites from the Highland Complex, Sri Lanka. Journal of Asian Earth Sciences, 28: 20–37.

Passchier, C.W., Trouw, R.A.J., Zwart, H.J. and Vissers, R.L.M. (1992). Porphyroblast rotation: eppur si muove? Journal of Metamorphic Geology, 10: 283–294.

Passchier, C.W. and Trouw, R.A.J. (2005) Microtectonics. Springer-Verlag, Berlin.

Raase, P. and Schenk, V. (1994) Petrology of granulite-facies metapelites of the Highland Complex, Sri Lanka: implications for the metamorphic zonation and the *P-T* path. Precambrian Research, 66: 265–294.

Raith, M., Faulhaber, S., Hoffbauer, R. and Spiering, B. (1991). Characterization of the high-grade metamorphism in the southern part of Sri Lanka in: The Crystalline Crust of Sri Lanka, Part I. Summary of Research of the German-Sri Lankan Consortium. Kröner, A. (Ed.), Professional Paper 5, Geological Survey Department, Sri Lanka, pp. 164 -178.

Ranaweera, L.V. and Kehelpannala, K.V.W. (2019) Mesoscopic to microscopic structures associated with the Wanni Complex/Highland Complex boundary shear zone in Sri Lanka. Journal of Geological Society of Sri Lanka, 20-2: 1-30.

Rosenfeld, J.L. (1970). Rotated garnets in metamorphic rocks, Special Paper 129, Geological Society of America.

Sajeev, K. and Osanai, Y. (2004). Ultrahigh-temperature metamorphism (1150°C, 12 kbar) and multistage evolution of Mg-, Al-rich granulites from the central Highland Complex, Sri Lanka. Journal of Petrology, 45: 1821–1844.

Sajeev, K., Williams, I.S. and Osanai, Y. (2010) Sensitive high-resolution ion microprobe U-Pb dating of prograde and retrograde ultrahigh-temperature metamorphism as exemplified by Sri Lankan granulites. Geology, 38: 971–974.

Santosh, M., Tsunogae, T., Malaviarachchi, S.P.K., Zhang, Z., Ding, H., Tang, L. and Dharmapriya, P.L. (2014) Neoproterozoic crustal evolution in Sri Lanka: Insights from petrologic, geochemical and zircon U–Pb and Lu–Hf isotopic data and implications for Gondwana assembly. Precambrian Research, 255: 1–29.

Schenk, V., Raase, P. and Schumacher, R. (1991) Metamorphic zonation and *P-T* history of the Highland Complex in Sri Lanka, in: The Crystalline Crust of Sri Lanka, Part I. Summary of Research of the German-Sri Lankan Consortium, Kröner, A. (Ed.), Professional Paper 5, Geological Survey Department, Sri Lanka, pp. 150–163.

Schoneveld, C. (1977) A study of some typical inclusion patterns in strongly paracrystalline-rotated garnets. Tectonophysics, 39: 453–471.

Schumacher, R., Schenk, V., Raase, P. and Vitanage, P.W. (2012) Granulite facies metamorphism of metabasic and intermediate rocks in the Highland Series of Sri Lanka, in: Ashworth, J.R., Brown, M. (Ed.), High-Temperature Metamorphism and Crustal Anatexis. The Mineralogical Society Series, pp. 235–271.

Spry, A. (1963) The origin and significance of snowball structure in garnet. Journal of Petrology, 4, 211–222.

Spry, A. (1969) Metamorphic Textures. Pergamon.

Touret, J.L.R., Huizenga, J.M., Kehelpannala, K.V.W. and Piccoli, F. (2019). Vein-type graphite deposits in Sri Lanka: The ultimate fate of granulite fluids. Chemical Geology, 508: 167–181.

Vernon, R.H., (1976). Metamorphic Processes. Allen & Unwin, London.

Vernon, R.H. and Collins, W.J. (1988). Igneous microstructures in migmatites. Geology, 16, 1126–1129.

Vernon, R.H. (2011) Microstructures of melt-bearing regional metamorphic rocks, in: van Reenen, D.D., Kramers, J.D., McCourt, S., Perchuk, L.L. (Eds.), Geological Society of America Memoirs

207. Geological Society of America, Boulder, Colorado, pp. 1–11.

Voll, G. and Kleinschrodt, R. (1991) Sri Lank: structural, magmatic, and metamorphic development of a Gondwana fragment, in: The Crystalline Crust of Sri Lanka, Part I. Summary of Research of the German-Sri Lankan Consortium. Kröner, A. (Ed.), Professional Paper 5, Geological Survey Department, Sri Lanka, pp. 22–51.

Williams, M.L. (1984) Sigmoidal inclusion trails, punctuated fabric development, and interactions between metamorphism and deformation. Journal of Metamorphic Geology, 12: 1–21.

Yoshida, M., Kehelpannala, K.V.W., Hiroi, Y. and Vitanage, P.W. (1990) Sequence of deformation and metamorphism of granulites of Sri Lanka. Journal of geosciences, Osaka City University 33: 69–107.

Zhao, G. and Cawood, P.A. (1999) Tectonothermal evolutionof the Mayuan assemblage in the Cathaysis Block: Implications for neoproterozoic collisional-related assembly of the South China craton. American Journal of Science, 299: 309-339.